Title:

Computational Analysis and Optimization of Cure process of Fiber Reinforced Polymer Composites for Reducing Process-Induced Warpage

Authors: Madhura Limaye[1], Dwayne Morgan[2], Gang Li[1*]

[1]Department of Mechanical Engineering, Clemson University, Clemson, SC - 29631, USA

[2]Touchstone Research Laboratory Inc., Triadelphia, WV 26059, USA

*Author to whom correspondence should be addressed. Electronic mail: gli@clemson.edu

Abstract

The cure processing of composite structures often suffers from residual stress inducement through internal and external sources. Two sources of residual stress development that have received considerable attention are mismatch of CTE and the cure shrinkage of resin. Experimental and numerical studies have shown that these process-induced stresses are directly influenced by the cure cycle the thermoset prepregs are subjected to. As a result, understanding the relationship between cure cycle parameters and induced stresses/deformations is critical for reducing residual stresses and restricting process-induced deformation within prescribed tolerances. In the present work, a methodology is developed to isolate the effects of individual cure cycle parameters by studying the evolution of the resin properties and identifying relationship between the cure cycle and the occurrence of two physical phenomena namely modulus development and cure shrinkage. The influence of these phenomena on the development of residual stresses and deformations through the underlying mechanisms of thermal and chemical shrinkage effects is investigated. Further, the effects of the cure cycle parameters on residual stresses and deformations are demonstrated by using three modified cure cycles. Finally, optimal cure cycle parameters that minimize the process-induced deformations are determined by using the process model and the NSGA-II genetic algorithm.

Keywords: *Cure behavior, Process simulation, Optimization, Residual stress, Process-induced deformation (PID), Thermoset composites, Finite element analysis*

Nomenclature

Point P	Initiation of polymerization
Point G	Gelation
Point V	Vitrification
PGV	Polymerization-Gelation-Vitrification
Instantaneous Tg	Instantaneous glass transition temperature
DoC or α	Degree of cure
CC	Cure cycle
ρ	Mass density
C_p	Specific heat
$\boldsymbol{k}$	thermal conductivity
H_R	resin heat of reaction
T	Temperature
$(A_i, \Delta E_i)$	experimentally determined cure kinetic model parameters (see Appendix A2)
R	universal gas constant
E_r	Resin Young's modulus
$E_{11}, E_{22},$ $E_{33}, G_{12}, G_{13}, G_{23},$ $\nu_{12}, \nu_{13}, \nu_{23}$	lamina elastic constants
CTE	coefficient of thermal expansion
CSC	Cure shrinkage coefficient
V_r^s	specific volumetric resin shrinkage
u	Laminate deformation
ε	Ply strain
σ	Ply stress
V_f	Fiber volume fraction
$\dot{Q}$	Resin Heat generation rate
$\frac{d\alpha}{dt}$	cure rate
ρ_r	resin density
U	strain energy
Ω_w	work done by body forces and surface tractions
$\boldsymbol{C}$	material stiffness matrix
$\boldsymbol{\varepsilon_0}$	internal strain vector

$\boldsymbol{\sigma_0}$	internal stress vector
$\boldsymbol{F_B}$	body force
$\boldsymbol{\varphi}$	surface traction
π_p	potential energy functional
$\boldsymbol{\delta}$	global displacement vector
$\boldsymbol{K}$	Global stiffness matrix
$\boldsymbol{F}$	Global force vector
$\boldsymbol{\varepsilon_{0_i}}$	internal strain vector in the ply principal directions
$\boldsymbol{\varepsilon_i^{th}}$	thermal strains in the ply principal directions
$\boldsymbol{\varepsilon_i^{ch}}$	cure shrinkage strains in the ply principal directions
E_r^0	modulus of the resin in the liquid phase
E_r^∞	modulus in the solid or fully cured state
α_1, α_2	DoC parameters for resin modulus development or cure shrinkage model
γ	Resin modulus development parameter
α_i	CTE of the composite lamina in the longitudinal and transverse directions.
$V_r^{s\infty}$	maximum volumetric shrinkage
ε_r^s	Resin shrinkage strains
CSC_i	cure shrinkage strain coefficients in the longitudinal and transverse directions
$\aleph t$	Non-dimensional curvature
l	cord length of the laminate
h	laminate rise
th	laminate thickness
Csh	Cure shrinkage
PID	Process induced deformation
S_1, S_2, and S_3	Linear segments of cure cycle
m_1, m_2, and m_3	Slopes of segments S_1, S_2, and S_3
t	Time

1 Introduction

Thermoset based fiber reinforced composite laminates are popularly processed by the cure process to produce structural parts. These structural parts have found extensive applications in aerospace and automotive industries [1,2]. A typical input to the cure process is a temperature and pressure cycle also commonly known as a cure cycle. The cure cycle initiates and enables completion of the cure reactions of the thermoset prepreg. The cure cycle also enables laminate consolidation and void reduction by excessive resin bleed-out and impregnation of fibers. However, the cure processing of composite structures often suffers from residual stress inducement through internal and external sources. The main sources of residual stress development in a composite laminate include a) mismatch of thermal expansion coefficients (CTE) at micro-level (fiber-resin interaction) and macro-level (ply-to-ply interaction), b) cure shrinkage of resin, c) temperature gradient through laminate thickness and, d) interaction between the composite laminate and the tool. For thin laminates, temperature gradients through thickness can be assumed to be negligible. Further, interaction between the laminate and tool are less critical for setups with thermally compatible tools. Thus, the two sources of residual stress development that have received considerable attention from researchers and industry alike are mismatch of CTE (thermal effects) and the cure shrinkage of resin (cure shrinkage effects) [3–9].

The residual stresses induced through these sources severely compromises the strength and adversely affect the performance of the composite laminate [9–13]. For example, these process-induced residual stresses have shown to cause matrix cracking which compromised its strength before mechanical loading [9,10]. In addition, cure process induced residual stresses were shown to have significant effect on the tensile strength of the matrix material [13]. Further, these residual stresses cause deformations in the laminate referred to as the process induced deformation (PID), and lead to deviations from the nominal dimensions. Such distorted laminate parts in assembly then give rise to mounting stresses [8,14–16]. Thus, minimizing or eliminating these process-induced residual stresses/deformation plays a key role in the manufacturing of high-quality composite structures. Experimental and numerical studies have shown that these process-induced stresses are directly influenced by the cure cycle the thermoset prepregs are subjected to [4,7,9,17]. As a result, determination of an optimal cure cycle is critical to reduce residual stresses and restrict deformation within prescribed tolerances. In the past, the determination of an optimal cure cycle was largely based on trial-and-error experimental methods [6–9,18]. Such an experimentally driven techniques are both expensive and time-consuming especially for large complex structures. Hence, there is a pressing need for adopting computational methods that adequately capture relevant physics of the cure problem to deliver optimized solutions for desired part quality.

In the past, computational models for cure simulation have been developed and solved using numerical methods such as the Finite Element method (FEM). These cure models mainly focused on predicting process induced stresses/deformation [4,19–25]. One notable investigation was conducted by Kravchenko et al. [4] where they studied effects of a modified cure cycle on the residual stresses/deformations. This modified cure cycle consisted of multi-linear heating steps leading to the cure temperature in contrast with a traditional cure cycle which consists of single linear heating step. Such a modified cure cycle was shown to cause interaction between the thermal and cure shrinkage effects of residual stress development. A reduction of stress-induced deformation was demonstrated which was attributed to the counteraction of cure shrinkage by thermal effects. However, the authors did not conduct an optimization study to determine the optimal parameters of the modified cure cycle to minimize stress-induced deformation.

Only few numerical studies are available in the literature that are focused on optimization of cure cycle parameters to minimize process induced residual stresses/deformations [9,19,26–28]. In a relevant study, Shah et al. [19] conducted a numerical investigation of cure process using a commercially available software COMPRO and optimized cure cycle parameters for an asymmetric laminate. Their objective was to achieve full cure in given time while minimizing the stress-induced deformation. They selected three (0.96, 0.98, 0.995) cure values and eight cure times to run a total of 24 optimization cases. They inferred that for a given cure value, longer cure times yielded lower deformation and a maximum of 10-12% reduction in stress-induced deformation was predicted. The study, however, did not investigate the effects of the individual cure cycle parameters and provide a physical explanation for the influence of these parameters on the process induced stress/deformation.

In the present work, through a theoretical and computational analysis of the rheology and thermomechanics of the curing laminate, we isolate the effects of the individual cure cycle parameters on the residual stress and process-induced-deformation. In the study, the laminate behavior during the cure process was studied and the relationship between the cure cycle and the occurrence of resin phase transition and thermomechanical interactions during cure process was identified. Further, the influence of these phenomena on the development of residual stresses/deformations through the underlying mechanisms of thermal and chemical shrinkage effects was established. In this manner, the mechanical behavior of laminates subjected to selected modified cure cycles was investigated and the effects of these modified cycles on the residual stress/deformation were demonstrated. Finally, the cure cycle parameters were optimized by using NSGA-II Genetic algorithm to fully exploit the competing mechanisms under play and achieve minimum stresses/deformation under given constraints.

2 Curing Physics

The essential role of the cure process of composites is to convert a low-density thermoset resin based composite prepreg to a high-density cross-linked laminated composite structure through polymerization reaction. During this conversion, the resin Youngs's modulus increases several orders of magnitude. This modulus development has a significant impact on the induced residual stress. For brevity, the increase in Young's modulus of the resin during the cure process will be referred to as modulus development in the rest of the paper. Further, as the density of the resin increases due to cross-linking, volume change occurs resulting in volumetric cure shrinkage in the resin. This also contributes to the residual stress developed in the laminate structure. Therefore, appropriate modeling of the resin behavior is important for accurate prediction of the cure induced residual stresses. For that purpose, the curing physics at the various stages of the cure process is described in this section and the rheological properties such as viscosity, glass transition temperature and cure kinetics are discussed.

As the first step into cure process, heat input is provided which turns the semi-solid prepreg into a viscous liquid. During this time, the liquid resin modulus is very low. The resin is free to flow and cannot support non-hydrostatic stress. As cure progresses, cross-linking of resin occurs. Cross-linking is the chemical reaction that creates 3-D cross-linked network from the short molecular chains of the resin. As a result, viscosity of the resin increases rapidly. This process is called Gelation. The laminate temperature is still very high at gelation; thus, the laminate behavior is visco-elastic which allows for stress decay. Cross-linking continues until vitrification is achieved. Vitrification point is reached when cross-linking is completed and the instantaneous glass transition temperature (Tg) of resin exceeds the laminate temperature. Beyond this point, the laminate mechanical behavior is fully elastic, and no stress-relaxation

is possible. Thus, the cure cycle is responsible for the transition of the phases (viscous, visco-elastic and elastic) and corresponding mechanical behavior in the laminate. Further investigation is necessary to reveal the relationship between the cure cycle and these phases as well as the effects on the mechanical behavior of the material including modulus development, thermal expansion, and cure shrinkage, we address this problem here via the development of Polymerization-Gelation-Vitrification (PGV) plots. Figure 1 illustrates such a PGV plot for a graphite epoxy laminate subjected to a two-step cure cycle. The two-step cure cycle consists of two heating periods, two dwell periods and a cooling period. The plot is explained by considering three distinctive phases and the laminate properties associated with each of the phases.

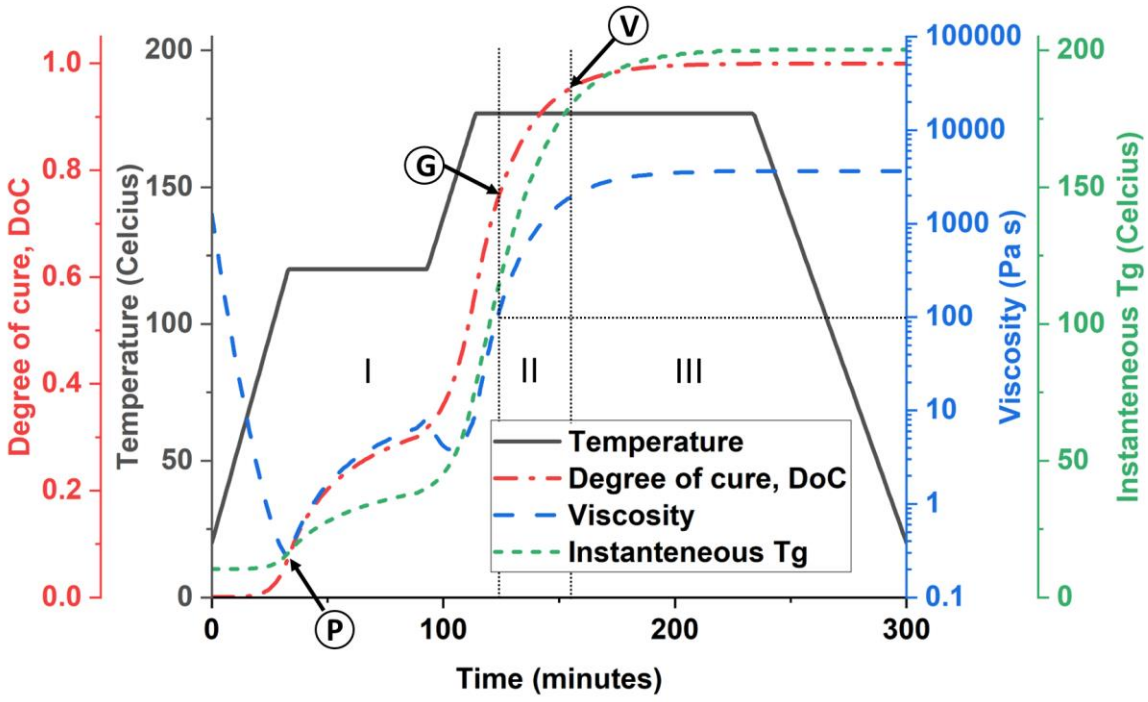

Figure 1. Property development for a laminate subjected to a two-step cure cycle (black curve) demonstrated through degree of cure profile (dash-dotted red curve), viscosity (dashed blue curve), and instantaneous glass transition temperature (Tg) profile (short dashed green curve). The cure cycle is divided into three phases: viscous phase (I), visco-elastic phase (II) and elastic phase (III).

As shown in Figure 1, Region I of the cure cycle is the viscous phase in which the polymer resin is in liquid state. The viscosity evolution as a function of the cure time is shown as the dashed blue curve in the PGV plot. The viscosity of resin drops to a minimum as the prepreg is heated to the first dwell temperature. This point marks initiation of polymerization reaction in the resin. Beyond this point, the viscosity increases quickly suggesting rapid cross-linking of resin. The degree of cure (DoC) corresponding to this point is marked with a point P. Gelation is considered to occur at the instance when viscosity reaches 100Pa.s. [29,30]. The DoC corresponding to the gelation point is marked with Point G in Figure 1. At gelation, resin becomes capable of supporting non-hydrostatic stress, hence it marks the beginning of modulus development. However, cure shrinkage initiates with cross-linking reactions. As a result, starting at point P, cure shrinkage is considered to occur. Point G marks the end of region I or the viscous phase of the resin.

Region II of the cure cycle is the visco-elastic phase. As cross-linking reaction continues throughout this phase, modulus development occurs during the entire time period of Region II. Similarly, cure shrinkage, which is linked to the cross-linking, occurs in this region as well. Thus, there is an overlap between the occurrence of modulus development and chemical shrinkage in this phase. The resin in this phase behaves as a visco-elastic solid and, as a result, stress relaxation is expected. The instantaneous Tg of the resin also evolves over the cure cycle shown by short-dashed green curve in the PGV plot. At an instance, the instantaneous Tg of resin crosses the laminate temperature. This is referred as vitrification point. The DoC corresponding to this point is marked with Point V. Beyond this point, cross-linking reaction ceases, and the associated modulus development and cure shrinkage is assumed to be completed. Thus, Point V marks the end of region II or the visco-elastic phase of the resin.

Region III of the cure cycle is the elastic phase. Beyond Point V, the modulus development and cure shrinkage are completed and the resin behaves as an elastic solid. Most of process-induced stress is developed in this region. This is due to the thermal contraction mismatch of the individual laminate plies during the cool down phase of the cure cycle considering that the stress relaxation becomes negligible. Thus, the PGV plot shown in Figure 1 illustrates the phases and associated behavior of the composite laminate as well as provides critical points to identify the occurrence of the modulus development and cure shrinkage.

3 Process modeling

The computational model for cure analysis is developed using a commercial FEA software ABAQUS along with a cure simulation tool COMPRO. The computational cure analysis is performed through a two-step simulation procedure. The two steps, namely the thermo-chemical step and stress-deformation step, are sequentially coupled and the results of the first step are used as input to the subsequent step. The detailed modeling approach, fundamental equations, and solution procedure for the two steps is provided in [31] and described in brief in this section. Additionally, the mathematical models of each step are described in this section. The assumptions of the analysis are (1) the laminate is void free; (2) the plies in the laminate are perfectly bonded; and (3) the laminate material is homogeneous, (4) fibers are transversely isotropic, and the matrix resin is isotropic. The effective thermal and mechanical ply properties are calculated using a micromechanics model [32] (see Appendix A3). The required inputs to the micromechanics model are the transversely isotropic fiber properties and isotropic resin properties. The inputs and outputs to each of the simulation steps is provided in **Error! Reference source not found.**.

Table 1. Inputs and outputs of the cure analysis steps

Analysis step	Inputs	Outputs
Thermo-chemical	mass density (ρ), specific heat (C_p) and thermal conductivity (k) of fiber and resin, resin heat of reaction (H_R) and an experimentally determined cure kinetic model parameters (A_i, ΔE_i)	Temperature (T) and DoC (α)
Stress-deformation	Temperature (T) and DoC (α) results from Thermo-chemical step, resin modulus (E_r), lamina elastic constants ($E_{11},\ E_{22},\ E_{33}, G_{12}, G_{13}, G_{23}, \nu_{12}, \nu_{13}, \nu_{23}$), coefficient of thermal expansion of fiber and resin (CTE), specific volumetric resin shrinkage (V_r^s)	Laminate deformation (u) ply strains (ε), and stresses (σ)

3.1 Thermo-chemical step

The thermo-chemical step considers cure of the resin as well as thermal interactions of the composite laminate with the surrounding air and the tool surface. The cure of the resin leads to an exothermic reaction and causes heat generation. The thermo-chemical analysis accounts for this internally generated heat. Thus, the thermo-chemical analysis seeks solutions of coupled heat transfer and cure kinetic equations. The system of governing equations is solved to obtain temperature and degree of cure (DoC) of the composite laminate. These models are described as follows.

3.1.1 Heat generation and transfer model

Fourier's heat conduction equation with heat generation is given by

$$\frac{\partial}{\partial t}(\rho C_p T) = \nabla(\boldsymbol{k}\nabla T) + \dot{Q} \tag{1}$$

where ρ is the density of the composite laminate, C_p is the specific heat, $\boldsymbol{k}$ is the anisotropic thermal conductivity and $\dot{Q}$ is the resin heat generation rate which is given by

$$\dot{Q} = \frac{d\alpha}{dt}(1 - V_f)\rho_r H_R \tag{2}$$

where α is the degree of cure which is a measure of the extent of cross-linking in the thermosetting polymer, $\frac{d\alpha}{dt}$ is the cure rate calculated using a cure kinetic model, V_f is the fiber volume fraction, ρ_r is the resin density and H_R is the resin heat of reaction/total heat evolved during the cure process. The governing equation (Eq. (1)) is solved by using the standard finite element method and the time integration is performed using the implicit backward Euler approach.

3.1.2 Cure Kinetic model

Various kinetic models have been developed to describe the cure rate of resin systems ($\frac{d\alpha}{dt}$) as a function of the DoC and temperature, the selection of model depends on the cure behavior of a particular resin. Two types of kinetic models have been developed using the model fitting approach: phenomenological models [33–36] and mechanistic models [37,38]. The phenomenological models are based on empirical rate laws and do not incorporate the details of the resin reaction. The mechanistic models take into account the details of the reaction such as species, concentration and other factors. For the epoxy material used in the present study, a phenomenological model is fit to express the cure kinetics as follows [39]

$$\frac{d\alpha}{dt} = \begin{Bmatrix} (B_1 + \alpha B_2)(1-\alpha)(\alpha_{crit} - \alpha), & \alpha \leq 0.3 \\ B_3(1-\alpha), & 1 \geq \alpha \geq 0.3 \end{Bmatrix} \tag{3}$$

where α is the degree of cure (DoC), $B_i = A_i e^{\frac{\Delta E_i}{RT}}$, where $A_i, \Delta E_i$ are the pre-exponential factors and activation energies, R is the universal gas constant and T is the temperature. The values of the model parameters are provided in Appendix A2. Note that the degree of cure (DoC) calculation (Eq. (3)) is performed separately from the temperature calculation (Eq. (1)) which means that the DoC and temperature are not considered as a coupled system. The time integration of Eq. (3) is performed by using the backward Euler method.

3.2 Stress-deformation step

The second step in the cure analysis computes deformations, residual strains, and stresses in the composite laminate. Similar to the thermo-chemical analysis, a finite element solution procedure is carried out for the stress-deformation analysis using the same discretized mesh. The temperature and DoC results computed from the thermo-chemical analysis are used as inputs in the stress-deformation analysis. The thermal, and mechanical effective lamina properties are calculated from the individual fiber and resin properties using the micromechanics equations. Next, process induced thermal and cure shrinkage strains are calculated by using the input temperature and DoC.

In the stress-deformation step, the variational principle was employed for structural analysis. Minimization of the potential energy functional leads to the governing equations and boundary conditions for a given structure. The potential energy functional can be expressed as [31]

$$\boldsymbol{\pi_p = U + \Omega_w} \tag{4}$$

where U is the strain energy of the systema and Ω_w is the work done by body forces and surface tractions during deformation. The detailed expression of the potential energy of the system is given by

$$\boldsymbol{\pi_p = \int_{\Omega} \left(\frac{1}{2}\varepsilon^T C\varepsilon - \varepsilon^T C\varepsilon_0 + \varepsilon^T \sigma_0\right) d\Omega - \int_{\Omega} u^T F_B d\Omega - \int_{\Gamma} u^T \varphi d\Gamma} \tag{5}$$

where $\boldsymbol{\varepsilon}$ is the strain field, $\boldsymbol{C}$ is the plain strain material stiffness matrix, $\boldsymbol{\varepsilon_0}$ is the internal strain vector, $\boldsymbol{\sigma_0}$ is the internal stress vector, $\boldsymbol{u}$ is the displacement field, $\boldsymbol{F_B}$ is the body force and $\boldsymbol{\varphi}$ is the surface traction. The internal strain vector in global axis $\boldsymbol{\varepsilon_0}$ is computed from internal strain vector in the ply principal directions $\boldsymbol{\varepsilon_{0_i}}$ defined as

$$\boldsymbol{\varepsilon_{0_i} = \varepsilon_i^{th} + \varepsilon_i^{ch} \qquad i = 1, 2} \tag{6}$$

The thermal, $\boldsymbol{\varepsilon_i^{th}}$ and cure shrinkage, $\boldsymbol{\varepsilon_i^{ch}}$strains are computed incrementally using material models described in Section 3.2.2 and Section 3.2.3.

The potential energy functional can be written in discrete form as:

$$\pi_p = \frac{1}{2}\boldsymbol{\delta^T K \delta - \delta^T F} \tag{7}$$

where $\boldsymbol{\delta, K, F}$ are the global displacement vector, stiffness matrix, and force vectors, respectively. Applying the principle of stationary potential energy

$$\frac{\partial \pi_p}{\partial \delta_i} = 0 \qquad for\ i = 1,2, \ldots\ldots, n \tag{8}$$

gives a system of algebraic equations of equilibrium

$$\boldsymbol{F = K\delta} \tag{9}$$

Finally, the global equations of equilibrium are solved to compute the laminate deformation. The laminate deformation is then post-processed to obtain ply strains and stresses. The models used in the solution procedure consist of the elastic constitutive model, thermal deformation model and chemical shrinkage model.

3.2.1 Elastic constitutive model

For the present study, a continuously linear elastic constitutive model (CHILE) is assumed for the fiber and resin. The elastic constants of the transversely isotropic composite are calculated at every time

step of the analysis by using the micromechanics model. The resin modulus can be defined as a function of resin temperature or cure or both. In this study, the expression of resin modulus development is DoC dependent and is given as follows [32]:

$$E_r = \begin{cases} E_r^0, & \alpha \le \alpha_1 \\ (1-\alpha_{mod})E_r^0 + \alpha_{mod}E_r^\infty + \\ \gamma\alpha_{mod}(1-\alpha_{mod})(E_r^\infty - E_r^0), & \alpha_1 \le \alpha \le \alpha_2 \\ E_r^\infty, & \alpha > \alpha_2 \end{cases} \quad (10)$$

where E_r^0 is the modulus of the resin in the liquid phase and E_r^∞ is the modulus in the solid or fully cured state. α_1 and α_2 are the DoC parameters for resin modulus development model. These parameters define bounds between which the modulus development takes place. As discussed in Section 2, modulus development is assumed to occur between points G and V in the PGV plot. Thus, α_1 is the degree of cure (DoC) corresponding to Point G in Figure 1while, α_2 is to the degree of cure (DoC) corresponding to Point V. γ is a parameter within the limits -1 and 1. The value of γ physically represents how rapidly the modulus develops initially until it reaches upper bound α_2. Finally, α_{mod} is calculated as $\alpha_{mod} = \frac{\alpha-\alpha_1}{\alpha_2-\alpha_1}$ such that it takes a value $0 \le \alpha_{mod} \le 1$.

3.2.2 Thermal deformation model

Thermal deformations are caused due to the mismatch of thermal expansion/shrinkage coefficients (CTE) of the fiber and the resin when exposed to temperature changes through the cure cycle. Accordingly, thermal expansion is caused during the heating periods while thermal shrinkage occurs during cool down. Both of these phenomena lead to significant thermal-induced deformation and contribute to the overall deformation of the structure. The incremental thermal strains are calculated as

$$\Delta\varepsilon_i^{th} = \alpha_i \Delta T \quad i = 1,2 \quad (11)$$

where CTE of the composite lamina, α_i in the longitudinal and transverse directions.

3.2.3 Chemical shrinkage model

Thermoset resins show reduction in specific volume during the cure process. The epoxy resin considered in the present study was estimated to undergo up to 3% volumetric chemical shrinkage. The resin volumetric shrinkage as a function of DoC is given by [32]:

$$V_r^s = \begin{cases} 0.0 & \alpha \le \alpha_1 \\ A\alpha_s + (V_r^{s\infty} - A)\alpha_s^2 & \alpha_1 \le \alpha \le \alpha_2 \\ V_r^{s\infty}, & \alpha \ge \alpha_2 \end{cases} \quad (12)$$

Again, α_1 and α_2 are the DoC parameters for cure shrinkage model. These parameters define bounds between which the cure shrinkage takes place. Referring to Figure 1, α_1 is the DoC corresponding to Point P while, α_2 is to the degree of cure DoC corresponding to Point V. Where $V_r^{s\infty}$ is the maximum volumetric shrinkage corresponding to 3% stain, A is a constant and α_s is given as $\alpha_s = \frac{\alpha-\alpha_1}{\alpha_2-\alpha_1}$. Resin shrinkage strains calculated from V_r^sas:

$$\varepsilon_r^s = (1 + V_r^s)^{1/3} - 1 \quad (13)$$

And incremental chemical shrinkage strains are given as

$$\Delta\varepsilon_i^{ch} = CSC_i \Delta\varepsilon_r^s \quad i = 1,2 \tag{14}$$

where chemical shrinkage strain coefficients, CSC_i in the longitudinal and transverse directions of the composite.

3.3 Model setup and validation: Cross-ply flat plate cure example

The modeling approach described in Section 3.1 and 3.2 was implemented for a flat rectangular laminate of dimensions 152mm×25mm×1.2mm with $[0_4/90_4]$ layup. The approach was numerically validated with a study in literature [19]. The laminate was divided into 8 sections through thickness and each section was a solid homogeneous ply. Figure 2 (b) shows the laminate geometry and unidirectional (UD) ply layup as well as the 0° and 90° plies orientations with respect to the global coordinate system. Each ply was defined with graphite/epoxy material system (material properties provided in Appendix A1). Two model setups were created for the cure analysis. First model setup was to perform thermo-chemical analysis while the second one was developed to perform stress-deformation analysis.

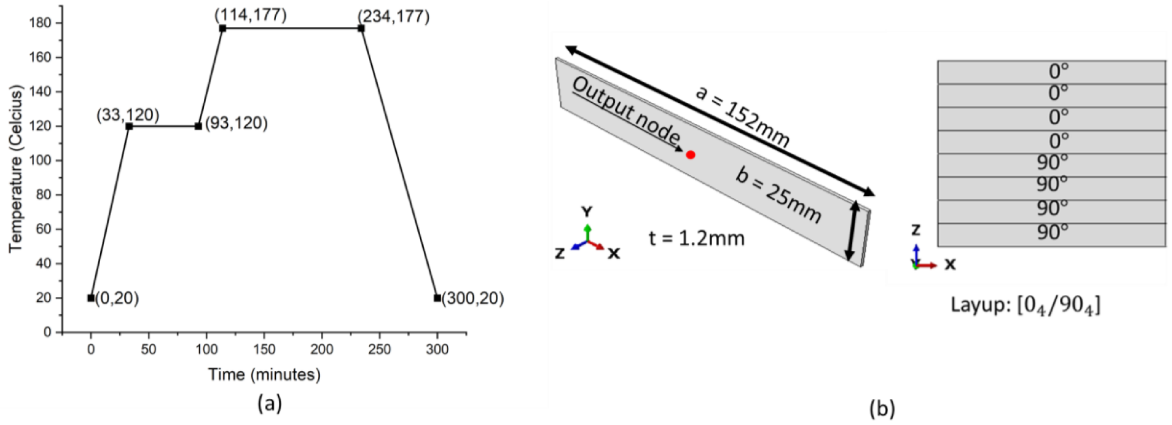

Figure 2. (a) Two-step cure cycle, (b) Geometry and layup of flat plate laminate used for the validation study.

3.3.1 Model setup for Thermo-chemical analysis

In the model setup, the cure cycle was assigned to all the surfaces of the laminate by defining a temperature boundary condition (BC). The cure cycle used for this study is shown in Figure 2 (a). The laminate was defined with an initial temperature BC of 20°C. Convection heat transfer with the surrounding air was not considered in the study. A mesh of 20-node solid elements (C3D20) was defined with a mesh grid of 30×6×8 elements in the laminate. Thus, each ply was modeled with 1 layer of elements through thickness. A transient thermo-chemical analysis was performed for the total time of 300 minutes as dictated by the cure cycle.

3.3.2 Model setup for stress-deformation analysis

The results obtained at the end of the thermo-chemical analysis namely temperature and degree of cure over the entire laminate were provided as inputs to the stress-deformation analysis. The modulus development and cure shrinkage parameters defined for the analysis are provided in Appendix A2. The model setup consisted of defining displacement boundary conditions to prevent any rigid body displacement. The edges defined with BC are shown in Figure 3. The edge (*0, y, 0*) was constrained for displacement in all directions whereas the edge (*a, y, 0*) was fixed in *y* and *z* displacements however free to

slide in *x* direction. The mesh remains same as the previous analysis. Transient analysis was performed for total time = 300min.

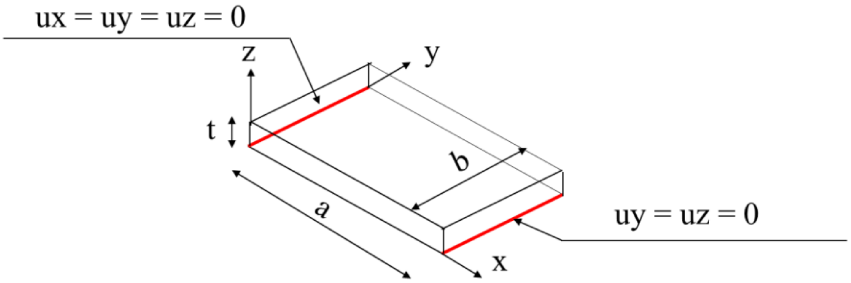

Figure 3. Boundary conditions defined in the stress-deformation step.

3.3.3 Thermo-chemical step validation

The results obtained from cure analysis were compared with the results from a numerical study from literature [19]. Accordingly, first the results of the thermo-chemical analysis namely temperature and degree of cure plots were compared. Figure 4 shows temperature on the primary Y axis and degree of cure on the secondary Y axis plotted versus time. The temperature profile was post-processed from the laminate at a node (see *Figure 2*(b)) and compared with [19]. Similarly, a DoC curve was obtained from the same node and plotted against the curve provided by [19]. Both the temperature and DoC curves showed good agreement.

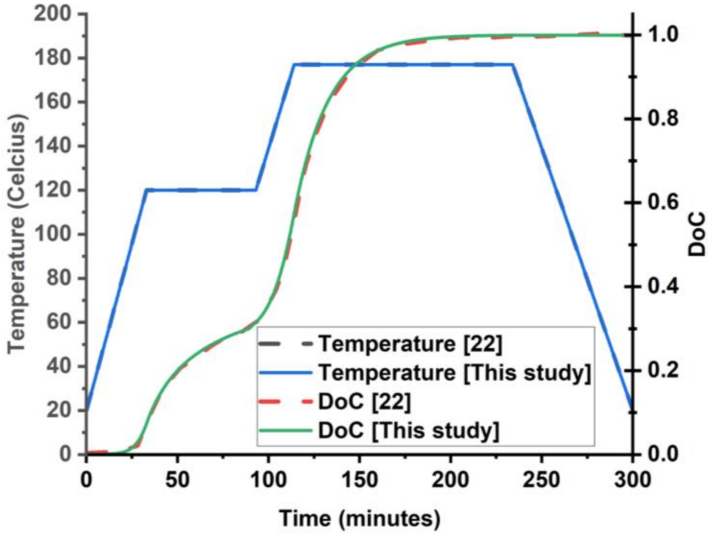

Figure 4. Comparison of temperature profiles and degree of cure curves from this work and Ref. [19]

3.3.4 Stress-deformation step validation

Displacement results were obtained from the stress-deformation analysis. The thermal and degree of cure history of the laminate induced two types of strains in the laminate namely thermal strains and chemical shrinkage strains. These strains induced throughout the cure cycle led to residual stresses in the laminate. For a symmetric laminate layup, the ply strains are balanced through thickness. However, for asymmetric layup used in the present study, the unbalanced strains led to curvature of the laminate. The residual stresses were proportional to the degree of curvature induced. The asymmetric layup considered in this study produced a curvature in the *x*-*z* and *y*-*z* planes respectively. A non-dimensional parameter was

defined to compare the curvatures obtained from experimental and numerical techniques as: $\aleph t = 2 \times h \times th/(l^2/4 + h^2)$, where l is the cord length of the laminate, h is the laminate rise and th is the laminate thickness. The non-dimensional curvatures obtained from this work were compared to the results of Ref. [19] in Table 2. Further, the displacement of the laminate in z-direction obtained from this work was plotted against the normalized length and width of the laminate and compared with the displacement results of Ref. [19] (see Figure 5). Both the non-dimensional curvatures and displacement comparisons showed good agreement.

Table 2. Comparison of non-dimensional curvatures calculated in this work and Ref. [19]

Non-dimensional curvature	**Shah et. al (10^{-4})**	**This work (10^{-4})**
x-z plane	43.92	42.42
y-z plane	44.16	40.47

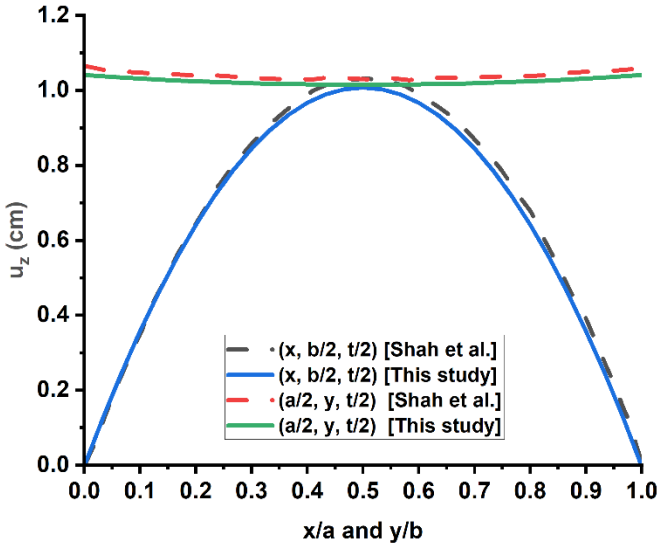

Figure 5. Comparison of uz displacement of the plate along normalized length and width of plate of this work and [19].

4 Effect of cure cycle parameters on composite residual stress and deformation

It is shown in Section 2 that modulus development and cure shrinkage are the two laminate behavior phenomena that significantly affect the residual stress development. Furthermore, it was understood from Section 3 that the thermal (CTE) and cure shrinkage (CSC) coefficients in the longitudinal and transverse directions of the plies contributed towards the development of thermal and cure shrinkage strains in the laminate. Thus, the two contributing components towards the total laminate residual strains/stress are identified as the Thermal effects and Cure Shrinkage (CSh) effects and are referred by these terms in the discussion to follow.

The Thermal effects are a function of temperature difference and DoC while the CSh effects are purely a function of crosslinking reaction of the resin which can be represented by the DoC. These effects become pronounced and cause PID only when modulus development occurs in the composite along the cure cycle. It is discussed in Section 3 that the modulus development phenomena occur between DoC values corresponding to points G and V while cure shrinkage occurs between points P and V as observed on the

PGV plot. Thus, it is shown from the PGV plot in Figure 1 that the two phenomena overlap only in Phase II. For a traditional isothermal dwell cure cycle, the cure shrinkage effects are dominant in the phase II. However, a modified cure cycle with a non-isothermal dwell period leads to an interaction between the Thermal and CSh effects and this interaction now dominates Phase II. The Thermal effects extent into Phase III for the modified cure cycle till the end of the cooling period. The effects of such a modified cure cycle on process-induced deformation (PID) are illustrated through three example cases.

For the three examples of modified cure cycles, the cure cycle parameters were reduced from the two-step cycle considered for model validation in the previous section, and a simplified one-step cure cycle shown in Figure 6 (a) was considered for illustration. Also, the geometry of the flat laminate was simplified, as shown in Figure 6 (b). The simplified geometry has dimensions 152mm × 25mm × 0.3mm and the laminate consists of 2 plies with layup 0/90.

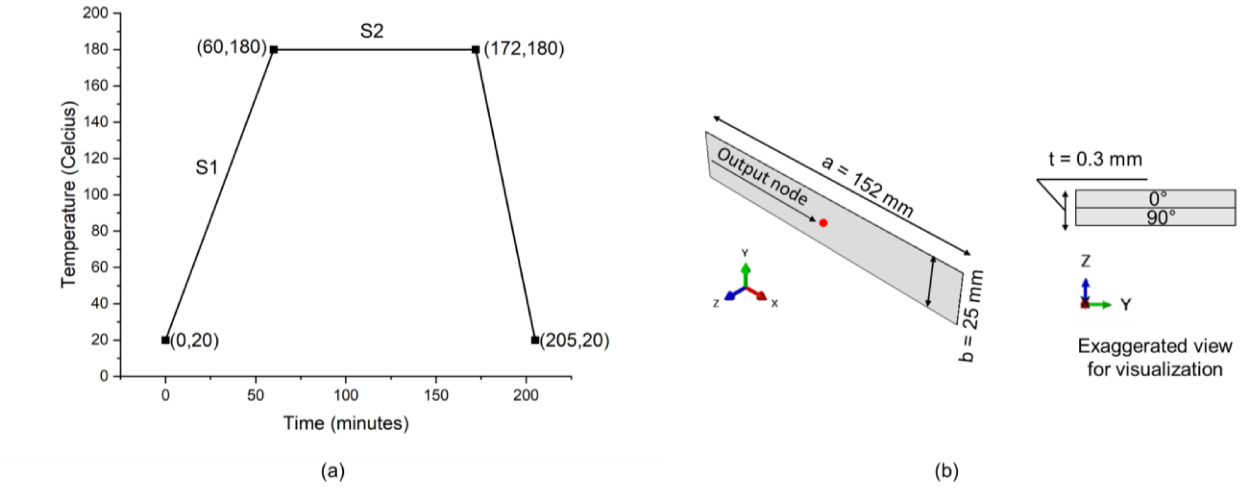

Figure 6. (a) One-step cure cycle, (b) simplified geometry with 2 plies in cross-ply layup used for the study

The modified cure cycles (see Figure 7) used in the present work were carefully chosen to exemplify the effects of cure cycle parameters on the PID. Each modified cycle has three linear segments, S_1, S_2, and S_3 with slopes m_1, m_2, and m_3, respectively. The slope of the last segment, m_3 and total cure time was maintained constant while the slopes of first two segments, m_1 and m_2, were varied. In Figure 7 (a), Modified cure cycle I has $m_1 > m_2$ where m_1, m_2 are positive numbers, Figure 7 (b) has $m_1 > m_2$ where m_1 is positive while m_2 is negative, lastly, Figure 7 (c) has $m_1 < m_2$, where m_1, m_2 are positive.

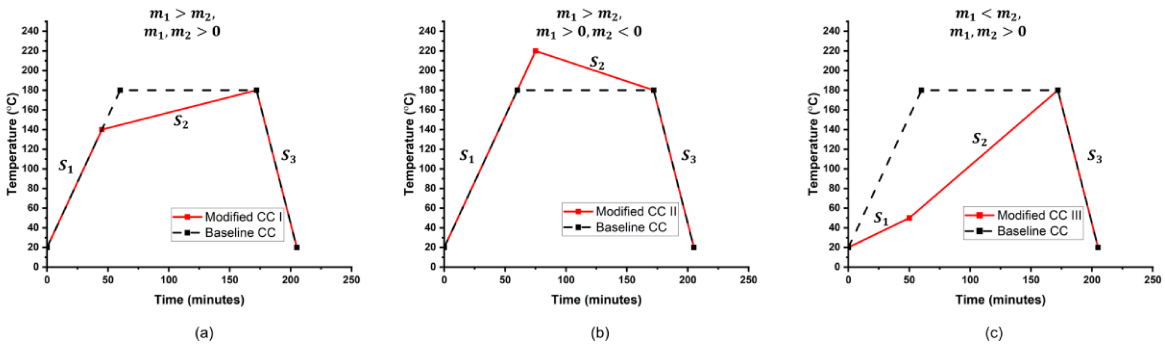

Figure 7. Three cases of one-step cure cycles considered for the present study

The cure simulations were performed using the validated cure model from Section 3.3. Accordingly, the thermo-chemical and stress-deformation analyses setup were adapted from the validation model. The baseline cure cycle used as thermal BC in the thermo-chemical analysis was replaced with the modified cure cycles. The temperature and DoC results of the thermo-chemical analysis were used to calculate viscosity and instantaneous glass transition temperature profiles according to the models provided in Appendix A2. With this information, PGV plot was constructed and the DoC parameters (α_1 and α_2) for the modulus development and cure shrinkage models were determined as defined in sections 3.2.1 and 3.2.3. These DoC parameters quantify the relationship between the cure cycle and the laminate mechanical behavior. These parameters were input to the models of the stress-deformation step. The stress-deformation analysis provided process-induced deformation results. The DoC parameters for all the baseline and the three modified cure cycle examples are provided in Table 3. It should be noted that the values of these parameters correspond to the location of points P, G and V on the PGV plots. The location of the P, G and V points are in turn dependent on the relationship between the cure cycle and the laminate behavior. Since this relationship differs for every cure cycle, the DoC parameters are different for the cure cycle cases considered in this study.

Table 3. DoC parameters for the baseline cure cycle case along with the three example cases

DoC parameter	Baseline		Case I		Case II		Case III	
	α_1	α_2	α_1	α_2	α_1	α_2	α_1	α_2
Cure shrinkage	0.0997	0.9554	0.0997	0.9369	0.0997	0.9999	0.103	0.8354
Modulus development	0.7569	0.9554	0.6561	0.9369	0.8785	0.9999	0.7498	0.8354

The PGV plots for the baseline and modified cure cycle I are provided in Figure 8. It was observed from Figure 8 (a) that the modulus development (G-V) occurs in the isothermal dwell period, while for modified cure cycle I, it occurs in the non-isothermal period as shown in Figure 8 (b). As a result, the modified cure cycle I causes interaction between the Thermal and CSh effects during phase II. Beyond Phase II (marked by point V), the Thermal effects are dominant till the end of the cooling period. The G and V points occur later in the cure process for the modified cure cycle I as compared to the baseline cure cycle case. This allows for a) resin squeeze in Phase I, b) part consolidation and stress relaxation in Phase II, c) PID reduction through Thermal effects in Phase III.

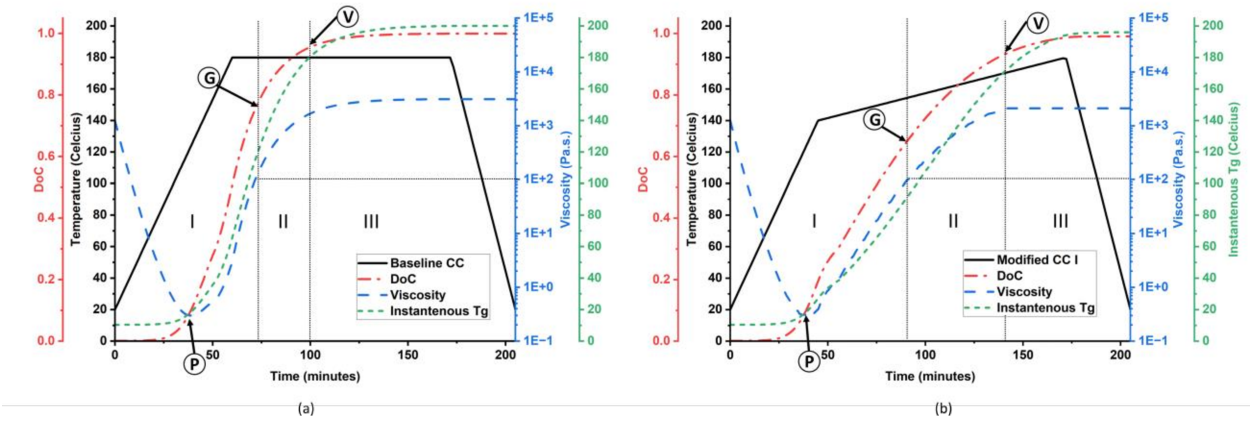

Figure 8. PGV plots for (a) baseline cure cycle and (b) modified cure cycle I

Figure 9 shows the deformation plots for the baseline cure cycle and modified cure cycle I. The evolution of PID at the output node shown in Figure 6 is plotted along with the temperature and DoC profiles to illustrate correlation between PID and DoC parameters. For the baseline cure cycle case, the CSh effects alone dominate between points G and V. While for the modified cure cycle I, there is thermal expansion due to positive temperature change, resulting in counteraction of the CSh effects by the Thermal effects. This observation is exemplified by isolating the Thermal and CSh effects and comparing them with the total deformation in Figure 10. Figure 10 shows that the Thermal effects up to cooling reduce the PID and help counteracting CSh effects in Phase II.

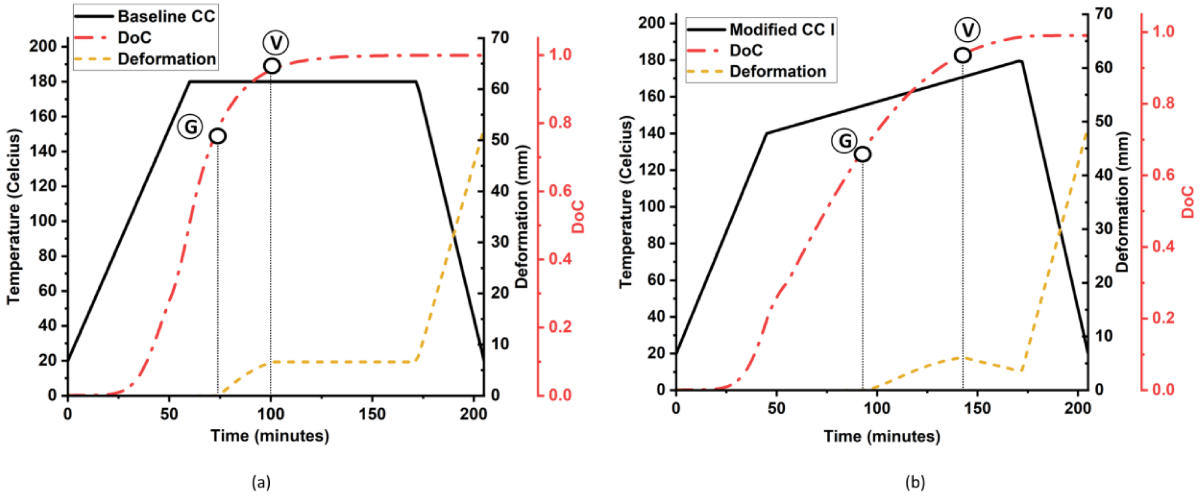

Figure 9. PID evolution plots for (a) baseline cure cycle and (b) modified cure cycle I

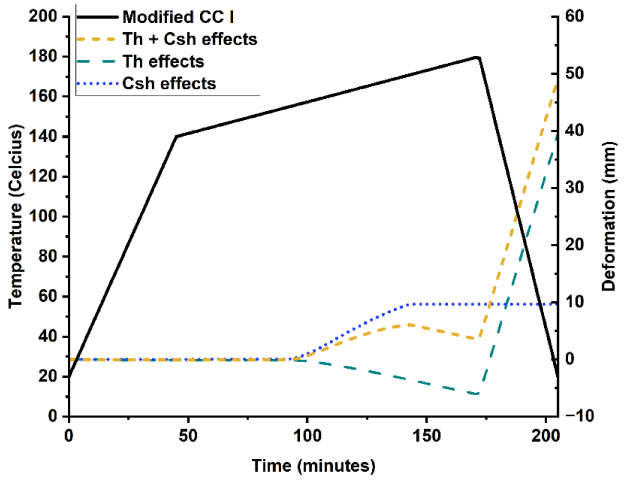

Figure 10. PID evolution with isolation of Thermal and Csh effects along with total deformation for the modified cure cycle I

Figure 11 shows the PGV plots for the modified cycles II and III. In case of the modified cure cycle II, the cure is carried out at a temperature much higher than the cure temperature (~ 180 °C for 3501-6 epoxy resin). Therefore, the DoC development takes place more rapidly compared to the baseline cure cycle. Vitrification point (Point V) is assumed to occurs at full cure (DoC ~= 0.99). The laminate is subjected to significant Thermal effects till the end of cooling. Regarding the physical behavior of the laminate, the

exposure to such high temperature could cause a) material degradation due to excessive heat generation, b) over consolidation due to excess resin flow especially for complex shaped structures. In case of the modified cure cycle III, the gelation (point G) is significantly delayed due to the low rate of heating which does not allow enough time for full cure. As a result, vitrification is not assumed to occur during the cure period. Laminates subjected to such cure cycles would lead to a) poor quality parts which are under consolidated and have compromised mechanical properties.

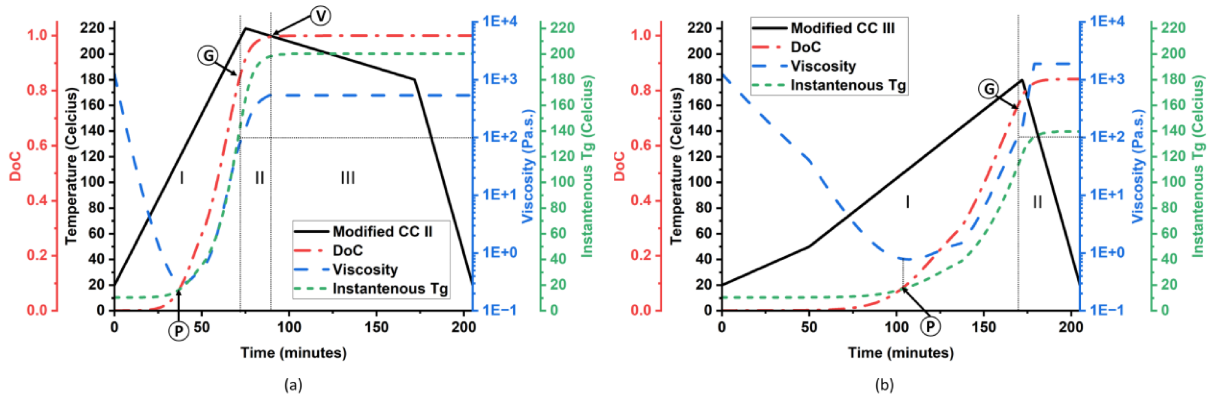

Figure 11. PGV plots for (a) modified cure cycle II and (b) modified cure cycle III

For the laminate deformation, Figure 12 shows the PID evolution plots for the modified cure cycles II and III. Since the slope m_2 for the modified cure cycle II is negative, the Thermal effects during Phase II lead to thermal shrinkage. The cumulative result of Thermal and CSh effects thus leads to a higher PID in this case. For the modified cure cycle III case, since the modulus development occurs very late in the cure process, the Thermal and CSh effects are negligible. Further, the final DoC is at 80% to full cure, as a result, the final PID magnitude is significantly lower as compared to the baseline cure cycle case. However, such a cure cycle is not desirable due to the lower DoC which is representative of poor mechanical properties.

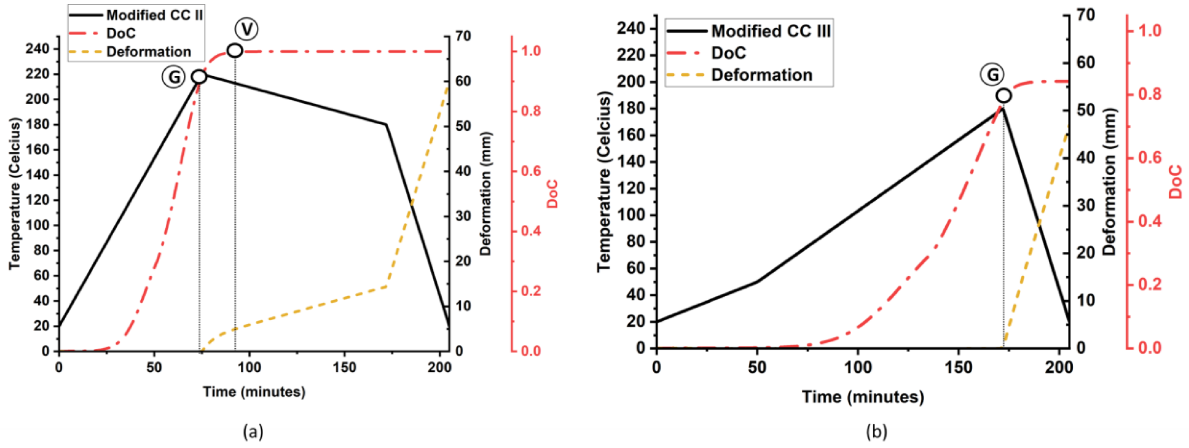

Figure 12. PID evolution plots for (a) modified cure cycle II and (b) modified cure cycle III

In summary, the selected cure cycle examples illustrate the effects of cure cycle parameters on the PID. For modified cure cycle I, the canceling interaction between Thermal and CSh effects was observed to cause reduction in PID and as a resulting this type of cure cycle was further investigated to fully exploit the effects of the competing mechanisms.

5 Optimization of Cure cycle Parameters

As demonstrated in the previous section, the cure cycle parameters have a significant effect on the rheology and the process-induced deformation (PID) of the composite structure. However, the question of what values of the slopes of cure cycle segments (m_1, m_2) will lead to minimal PID of the laminate remains. In addition, the objective of minimizing PID must be accompanied by the physical constrain of ensuring a full cure of the composite structure within reasonable amount of time. In this section, we define and solve a multivariable optimization problem to minimize the laminate PID.

5.1 Optimization problem and cases

Objective: $Minimize(u)$

Contraints: 1. $DoC \geq x - 0.0005,\ x = 0.990, 0.995$

2. $m_1 > m_2,\ m_1, m_2 > 0$

Inputs: $t,\ T$

Outputs: 1. $m_1 - m_2$

2. DoC

3. u

The optimization problem was set up in ModeFRONTIER software. A python script was used to integrate the ABAQUS-COMPRO cure simulation with the ModeFRONTIER environment. The design variables of the optimization problem were the coordinates of point A (*t, T*) of the point encircled in Figure 13. The location of this point in the *t*-*T* plane controlled the slopes (m_1 and m_2) of segments S_1, and S_2 as well as the interaction between Thermal and CSh effects. The constraints imposed on the optimization process ensured that (1) cured composite structure is acceptably cured (DoC >= 0.990) and (2) modified cure cycle designs always result in counteraction of the CSh and Thermal effects to reduce PID ($m_1 > m_2$, & $m_1, m_2 > 0$). The genetic algorithm NSGA-II was used to solve the optimization problem [40].

Genetic algorithms, in general, overcome the limitations of the classical techniques (direct or gradient-based algorithms) such as dependence on the chosen initial solution and getting stuck to a suboptimal solution. Among the different genetic algorithms, NSGA-II has some unique features that include: 1) use of elitist principles that is the elites of a population are given the opportunity of being carried in the next generation, 2) use of a mechanism called crowding distance sorting to preserve diversity in the search space, 3) use of another technique called the non-dominated sorting where solution fronts are created and ranked based on a domination criteria. The non-dominated solution fronts of better ranks are emphasized for creating the next generation. NSGA-II algorithm has the following procedure [40]: In the first step, offspring population having the same size as the parent population is created through crossover, elitism or mutation. The combination of parent and offspring populations are classified into fronts using the non-dominated sorting technique. These fronts are ranked according to an ascending level of non-domination. The best ranked fronts are then carried into the new population which are the same size as the previous population. If a particular front cannot be carried entirely to the new population, the crowd sorting technique is used. Crowd distance sorting is based on determination of density of solutions around each solution and assigning preference to less dense solutions. In the final step, offspring population is selected from the new population based on front ranking or crowd distance using crossover and mutation operators. The procedure is repeated for several generations till convergence is achieved.

In this work, the initial population/ designs were defined to be 100. The optimization algorithm was run for 10 generations to perform a total of 1000 evaluations.

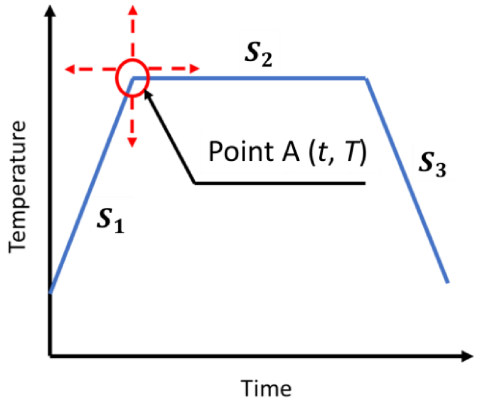

Figure 13. Cure cycle parameters: coordinates of point A (t, T) used for optimization study

Four optimization cases namely R11, R12, R21 and R22 were considered as shown in Table 4. The selection of the cases was based on two considerations: (1) as input variable t is the time for heating the composite laminate in the cure cycle, two values of t=1 min for cases R11, R12 and t=10min for cases R21, R22 were selected for evaluation considering the manufacturing efficiency and feasibility. An upper bound of 110 min was defined for t whereas T was defined such that 125<= T <=180, since the design samples outside these bounds had shown to be infeasible in trial runs; (2) the final value of DoC must be higher than 0.99 which is considered full cure of the resin for sufficient modulus development and final properties of the composite structure. Hence two values of DoC=0.990 for cases R12, R22 and DoC=0.995 for cases R11, R21 were considered for evaluation of the optimized cure cycle.

Table 4. Optimization cases performed for the present study

Cases	DoC	Range of t (min)	Range of T (°C)
R11	> 0.995	1-110	125-180
R12	> 0.990	1-110	125-180
R21	> 0.995	10-110	125-180
R22	> 0.990	10-110	125-180

5.2 Optimization results and discussion

The results obtained from the optimizer were assessed with the help of post-processing tools in ModeFRONTIER such as history plots and bubble charts. Several charts for case R12 are provided in the Appendix A4. Table 5 provides the optimal cure cycle parameters for the four cases (R11-R22) and the baseline case. The optimal parameters of R11 and R12 are (1.001min, 134.36°C) and (1.059min, 134.78°C) respectively, while for R21 and R22 cases values are (10.230min, 135.76°C) and (10.209min, 135.32°C) respectively. Table 5 also provides the final degree of cure values and deformation magnitudes for all cases.

Figure 14(a) shows the plots of the optimal cure cycles R11 and R21 along with the baseline cure cycle. Figure 14(b) shows the deformation history plots for the optimal cure cycles R11 and R21 along with the baseline case. A discussion related to the results obtained from the optimization is as follows:

- As shown in Table 5 the optimal values of *t* and *T* for the R11 and R12 cases are nearly the same. The R11 optimization problem was defined with a constraint such that all evaluated cases with $DoC \geq 0.995$ were considered feasible, while in the R12 optimization problem the range of the design space was increased such that all cases with $DoC \geq 0.990$ were considered feasible. However, since the optimal parameters lead to a final degree of cure of 0.996, the increase in the design space did not change the optimum. Similarly, negligible change was observed in the optimum for the R21 and R22 cases. This result implies that the optimal point A guarantees full cure of the resin.
- The total deformation for the baseline cycle is 52.207mm while for the R11 and R12 cases it is 46.988mm and 47.003mm respectively. The reduction in deformation for the R11 and R12 optimal cure cycles compared to the baseline cure cycle was about 10%. For the R21 and R22 optimal cure cycles, total deformation is 47.683mm and 47.664mm, respectively, which amounted to a reduction of 8.7% from the baseline case.
- The results of all optimization cases show that the optimal values of input parameter *t* are almost equal to the defined lower limits 1min and 10min respectively. This suggests that the optimizer maximized the non-isothermal dwell time thus achieving maximum interaction between the Thermal and CSh effects. The results also show that increasing the lower limit of *t* from 1min to 10min led to an increase in the PID, which means, for a fixed total cure time, increasing the initial heating time (*t*) directly increases the PID. Therefore, considering the manufacturing feasibility, a minimum possible value of *t* should be chosen to achieve minimum PID.
- The total deformation was broken down into two parts, deformation before cooling and deformation post cooling. The results for both these parts are provided in the Table 5. These two parts are illustrated in the cure cycle and deformation history plots in Figure 14. The predicted deformation before cooling for the baseline cycle is 6.559mm which accounts for 12.56% of the total deformation. While for R11 and R12 cycles, the deformation before cooling is 1.359mm and 1.424mm, respectively, which corresponds to an average of 2.95% of the total deformation. For the R21 and R22 cases, the obtained values for deformation before cooling are 2.600mm and 2.217mm, respectively, which gives an average of 5.05% of the total deformation.
- The significant decrease in deformation before cooling for the R11 through R22 cases compared to the baseline case can be attributed to the interaction between thermal expansion and cure shrinkage effect. The thermal expansion cancels a large part of the cure shrinkage in the optimal cure cycles and further helps reduce the deformation up to cooling.
- It is observed in Table 5 that the deformation magnitudes post cooling are not identical for all cases given that the temperature change for cooling is the same. This is because the final composite modulus at the end of modulus development depends on the final degree of cure achieved. As the final degree of cure for the considered cases are different, minor difference is seen in the deformation post cooling.

Table 5. Results of optimization cases

Case	*t* *(min)*	*T* *(°C)*	DoC	Deformation before cooling (mm)	% deformation before cooling	Deformation post cooling (mm)	Total deformation (mm)
Baseline	*60*	*180*	1.000	6.559	12.56	45.648	52.207
R11	*1.001*	*134.36*	0.996	1.359	2.89	45.639	46.988
R12	*1.059*	*134.78*	0.996	1.424	3.02	45.579	47.003
R21	*10.230*	*135.76*	0.9955	2.600	5.45	45.083	47.683
R22	*10.209*	*135.32*	0.9953	2.217	4.65	45.447	47.664

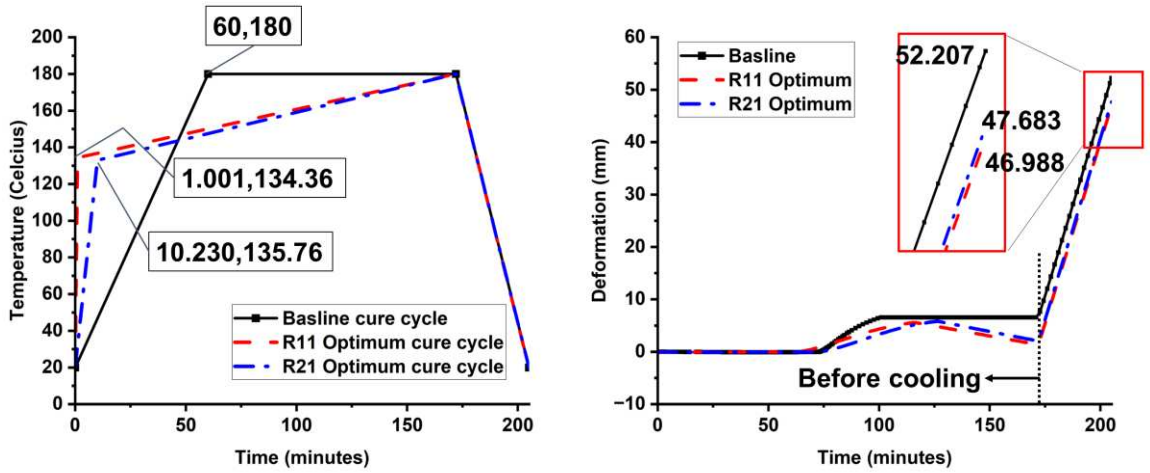

(a) (b)

Figure 14. a) Optimal cure cycles R11 and R21 along with the baseline cure cycle, b) deformation history plots for optimal cure cycles R11 and R21 along with the baseline cure cycle case.

5.3 Study of non-linear cure cycles

In the above optimization study, the cure cycles considered were multi-linear in nature. Such linear variation of temperature limits the design space of the cure cycle profile. In this section, the cure cycle design space was enlarged by allowing a non-linear increase of temperature. Such temperature profiles are referred to as non-linear cure cycles. These non-linear cure cycles were constructed using the Bezier curve generation method. The Bezier curve generation method requires multiple control points for construction which were obtained from the multi-linear cure cycles. To investigate the effect of temperature nonlinearity, two multi-linear cure cycles were considered for comparison: (1) the baseline cure cycle and (2) the optimized cure cycle. For each multi-linear cure cycle, three Bezier curves were constructed with 3, 5 and

7 control points, respectively, (see Figure 15 (a) and (c)). Cure simulations were performed for each of these non-linear cure cycles to obtain displacement evolution plots. Figure 15 (b) and (d) show the displacement evolution plots for non-linear cure cycles generated from baseline cure cycle and optimized cure cycle respectively.

Table *6* provides quantitative results for the nonlinear temperature profiles generated from baseline cure cycle. The

Table *6* shows that the 3-point Bezier cure cycle generated from baseline cure cycle reduced PID by 2.65% whereas the amount of reduction in PID dropped to 2.44% and 1.04% for 5-point and 7-point cases, respectively. The reduction in PID can be explained by the fact that in case of the non-linear Bezier curves, the non-isothermal heating (temperature increase) lead to counteraction of CSh effects by Thermal effects which reduces the overall deformation. While the trend of the results can be understood by observing in Figure 15 (a) that with increase in the number of control points from 3 to 7, the curves fit closer to the baseline multi-linear cycle and the difference in slopes reduces. As a result, the 7-point Bezier curve behaves more like the baseline cure cycle as compared to the 5-point and 3-point curves.

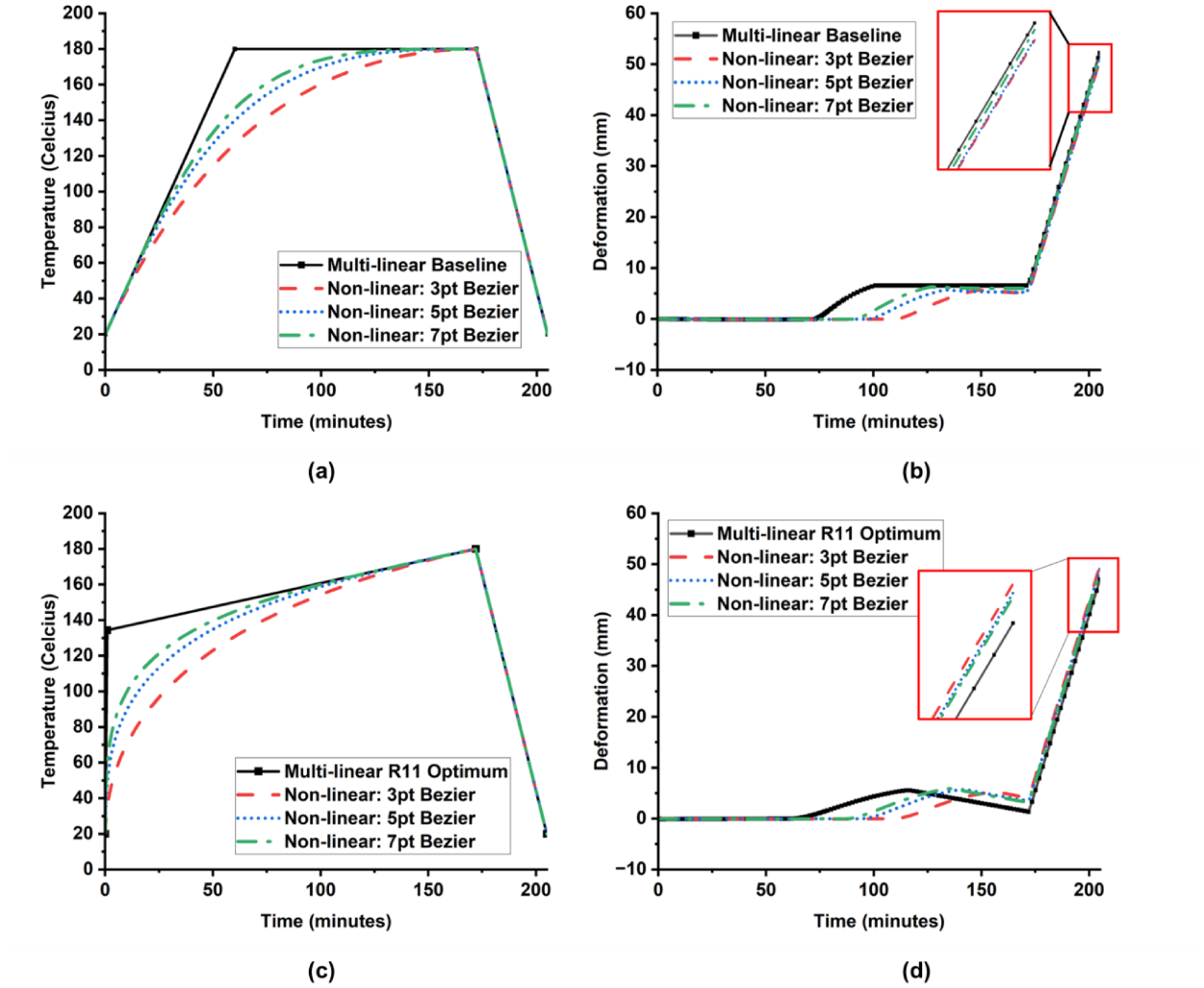

Figure 15 (a) Bezier curves representing non-linear cure cycles fitted using baseline multi-linear cure cycle, (b) PID evolution plots for cure cycles in (a), (c) Bezier curves representing non-linear cure cycles fitted using optimized multi-linear cure cycle, (d) PID evolution plots for cure cycles in (c)

Table 6. Process-induced deformation in non-linear cure cycle cases as compared to the baseline cure cycle case

Cure cycle	DoC	Deformation (mm)	% difference in deformation as compared to baseline cure cycle (positive: decrease, negative: increase)
Baseline	0.999	52.207	
Bezier 3-pt	0.992	50.821	2.65
Bezier 5-pt	0.996	50.931	2.44
Bezier 7-pt	0.998	51.66	1.04

Table 7 provides quantitative results for the nonlinear temperature profiles generated from optimized multi-linear cure cycle. The results show increase in PID by 5.76% for 3-point, 4.43% for 5-point and

3.83% for 7-point Bezier cure cycles. These results are in contrast to the deformation results of the nonlinear temperature profiles generated from the baseline cure cycle shown in Table 6. This is due to the fact that the optimized cure cycle consists of optimized slopes of heating segments which produce maximum interaction between the Thermal and CSh effects resulting in minimum PID. The nonlinear cure cycles generated from the optimized cure cycle do not have optimized slopes, leading to higher magnitude of PID. The trend of the results also follows the reasoning that the 7-point curve matches more closely to the optimized cure cycle as compared to the 5-point and 3-point curves. The results imply that the PID increase diminishes when the nonlinear cure cycle asymptotically approaches the optimized multi-linear curve cycle, and therefore, the optimized multi-linear curve cycle is the global optimal solution.

Table 7. Process-induced deformation in non-linear cure cycle cases as compared to the optimized cure cycle case

Cure cycle	DoC	Deformation (mm)	% difference in deformation as compared to optimized cure cycle (positive: decrease, negative: increase)
Optimized	0.996	46.988	
Bezier 3-pt	0.985	49.698	-5.76
Bezier 5-pt	0.991	49.073	-4.43
Bezier 7-pt	0.993	48.791	-3.83

6 Conclusion

A cure process induced deformation analysis considering the relevant physics such as heat transfer, cure kinetics and composite laminate mechanics was carried out for a 3D flat laminate structure. The cure model was validated with a numerical model available in literature. In this work, a methodology was developed to isolate the effects of the individual cure cycle parameters by studying the evolution of the resin properties including the viscosity, degree of cure, and instantaneous Tg. Accordingly, the relationship between the cure cycle and the modulus development and cure shrinkage phenomena during cure process was determined by using PGV plots. Further, the influence of these physical behavior on the development of residual stresses/deformations through the thermal and chemical shrinkage effects was established. The mechanical behavior of laminates subjected to three selected modified cure cycles was investigated and the effects of these modified cycles on the residual stress/deformation were demonstrated. It was shown that the cure cycle with rate of heating higher in the first ramp compared to the second ramp produced counteraction of CSh effects by Thermal effects resulting in lower PID. Next, an optimization problem was setup to determine the optimal cure cycle parameters with the objective to minimize the process induced deformation. The deformation results of the optimal cure cycles showed a meaningful (8-10%) reduction when compared to the baseline/manufacturer recommended cure cycle. Finally, nonlinear cure cycles with

Bezier temperature curves were investigated. It was shown that the nonlinear cure cycle produces the minimal PID when it asymptotically approaches the optimized multi-linear curve cycle. Therefore, it is concluded that the optimized multi-linear curve cycle is the global optimal solution.

Acknowledgement
The authors are thankful to NASA Langley Research Center (LaRC) and Touchstone Research Laboratory Inc. for financial support through Phase I and Phase II STTR Grant Funding according to Contract 80NSSC21C0021. This work is partially supported by the National Science Foundation under Grant No. 2244342.

Data Availability
Data will be made available upon request.

References

[1] McIlhagger A, Archer E, McIlhagger R. 3 - Manufacturing processes for composite materials and components for aerospace applications. In: Irving P, Soutis C, editors. Polymer Composites in the Aerospace Industry (Second Edition) [Internet]. Second Edi. Woodhead Publishing; 2020. p. 59–81. Available from: https://www.sciencedirect.com/science/article/pii/B9780081026793000034.

[2] Pradeep SA, Iyer RK, Kazan H, et al. Automotive Applications of Plastics: Past, Present and Future. In: Kutz M, editor. Applied Plastics Engineering Handbook: Processing, Materials, and Applications. 2nd ed. Oxford: Elsevier; 2017. p. 651–674.

[3] Gopal AK, Adali S, Verijenko VE. Optimal temperature profiles for minimum residual stress in the cure process of polymer composites. Compos Struct. 2000;

[4] Kravchenko OG, Kravchenko SG, Pipes RB. Cure history dependence of residual deformation in a thermosetting laminate. Compos Part A Appl Sci Manuf. 2017;

[5] Sreekantamurthy T, Hudson TB, Hou TH, et al. Composite cure process modeling and simulations using compro® and validation of residual strains using fiber optics sensors. Proceedings of the American Society for Composites - 31st Technical Conference, ASC 2016. 2016.

[6] Genidy MS, Madhukar MS, Russell JD. New method to reduce cure-induced stresses in thermoset polymer composites, Part II: closed loop feedback control system. J Compos Mater. 2000;34.

[7] Madhukar MS, Genidy MS, Russell JD. New method to reduce cure-induced stresses in thermoset polymer composites, Part I: test method. J Compos Mater. 2000;34.

[8] Russell JD, Madhukar MS, Genidy MS, et al. New method to reduce cure-induced stresses in thermoset polymer composites, Part III: Correlating stress history to viscosity, degree of cure, and cure shrinkage. J Compos Mater. 2000;34.

[9] White SR, Hahn HT. Cure Cycle Optimization for the Reduction of Processing-Induced Residual Stresses in Composite Materials. J Compos Mater. 1993;27.

[10] Hahn HT. Residual Stresses in Polymer Matrix Composite Laminates. J Compos Mater. 1976;

[11] Agius SL, Joosten M, Trippit B, et al. Rapidly cured epoxy/anhydride composites: Effect of residual stress on laminate shear strength. Compos Part A Appl Sci Manuf. 2016;

[12] Zhao LG, Warrior NA, Long AC. A micromechanical study of residual stress and its effect on transverse failure in polymer-matrix composites. Int J Solids Struct. 2006;

[13] Li C, Zobeiry N, Keil K, et al. Advances in the characterization of residual stress in composite structures. International SAMPE Technical Conference. 2014.

[14] Ersoy N, Garstka T, Potter K, et al. Modelling of the spring-in phenomenon in curved parts made of a thermosetting composite. Compos Part A Appl Sci Manuf. 2010;

[15] Kravchenko OG, Kravchenko SG, Pipes RB. Chemical and thermal shrinkage in thermosetting prepreg. Compos Part A Appl Sci Manuf. 2016;

[16] Gigliotti M, Wisnom MR, Potter KD. Development of curvature during the cure of AS4/8552 [0/90] unsymmetric composite plates. Compos Sci Technol. 2003;

[17] Sarrazin H, Kim B, Ahn SH, et al. Effects of Processing Temperature and Layup on Springback. J Compos Mater. 1995;

[18] Purslow D, Childs R. Autoclave moulding of carbon fibre-reinforced epoxies. Composites. 1986;

[19] Shah P, Halls V, Zheng J, et al. Optimal cure cycle parameters for minimizing residual stresses in fiber-reinforced polymer composite laminates. J Compos Mater [Internet]. 2018;52:773–792. Available from: http://journals.sagepub.com/doi/10.1177/0021998317714317.

[20] Sun L, Wang J, Ni A, et al. Modelling and experiment of process-induced distortions in unsymmetrical laminate plates. Compos Struct. 2017;182.

[21] Liu X, Guan Z, Wang X, et al. Study on cure-induced residual stresses and spring-in deformation of L-shaped composite laminates using a simplified constitutive model considering stress relaxation. Compos Struct. 2021;272.

[22] Benavente M, Marcin L, Courtois A, et al. Numerical analysis of viscoelastic process-induced residual distortions during manufacturing and post-curing. Compos Part A Appl Sci Manuf. 2018;107.

[23] Ersoy N, Garstka T, Potter K, et al. Modelling of the spring-in phenomenon in curved parts made of a thermosetting composite. Compos Part A Appl Sci Manuf. 2010;41.

[24] Chen W, Zhang D. A micromechanics-based processing model for predicting residual stress in fiber-reinforced polymer matrix composites. Compos Struct. 2018;204.

[25] Li D, Li X, Dai J. Process modelling of curing process-induced internal stress and deformation of composite laminate structure with elastic and viscoelastic models. Applied Composite Materials. 2017;25.

[26] Wang Q, Yang X, Zhang X, et al. Effect of cure cycles on residual stresses in thick composites using multi-physics coupled analysis with multiple constitutive models. Mater Today Commun. 2022;32:104094.

[27] Hui X, Xu Y, Zhang W, et al. Multiscale collaborative optimization for the thermochemical and thermomechanical cure process during composite manufacture. Compos Sci Technol. 2022;224:109455.

[28] Li X, Han X, Duan S, et al. A Two-Stage Genetic Algorithm for Molding Parameters Optimization for Minimized Residual Stresses in Composite Laminates During Curing. Applied Composite Materials. 2021;

[29] Roller MB. Characterization of the time-temperature-viscosity behavior of curing B-staged epoxy resin. Polym Eng Sci. 1975;15.

[30] Loos AC, Springer GS. Curing of Epoxy Matrix Composites. J Compos Mater. 1983;17.

[31] Johnston A a. An integrated model of the development of process-induced deformation in autoclave processing of composite structures. University of British Columbia; 1997.

[32] Bogetti TA, Gillespie JW. Process-Induced Stress and Deformation in Thick-Section Thermoset Composite Laminates. J Compos Mater. 1992;26:626–660.

[33] Boey FYC, Song XL, Rath SK, et al. Cure reaction for modified diallylbisphenol A/diaminodiphenylsulfone/bismaleimide. J Appl Polym Sci. 2002;85.

[34] Morgan RJ, Shin EE, Rosenberg B, et al. Characterization of the cure reactions of bismaleimide composite matrices. Polymer (Guildf). 1997;38.

[35] Abbate M, Martuscelli E, Musto P, et al. Thermosetting bismaleimide/reactive rubber blends: Curing kinetics and mechanical behavior. J Appl Polym Sci. 1997;65.

[36] Goodwin AA. The curing kinetics of a modified bismaleimide. Polym Int. 1993;32.

[37] Phelan JC, Sung CSP. Cure characterization in bis(maleimide)/diallylbisphenol A resin by fluorescence, FT-IR, and UV-reflection spectroscopy. Macromolecules. 1997;30.

[38] Hopewell JL, George GA, Hill DJT. Quantitative analysis of bismaleimide-diamine thermosets using near infrared spectroscopy. Polymer (Guildf). 2000;41.

[39] Woo IL, Loos AC, Springer GS. Heat of Reaction, Degree of Cure, and Viscosity of Hercules 3501-6 Resin. J Compos Mater. 1982;16.

[40] Deb K, Pratap A, Agarwal S, et al. A fast and elitist multiobjective genetic algorithm: NSGA-II. IEEE Transactions on Evolutionary Computation. 2002;6.

Appendix

A1. Material properties of fiber and resin

	Material property	**Graphite fiber**		**Epoxy resin**	
1	Mass density $\rho\ (kg/m^3)$	1790		1260	
2	Specific heat $C_p\ (J/kg-K)$	712		1260	
3	Thermal conductivity $k\ (W/m-k)$	k_l = 26	k_t = 2.6	0.167	
4*	Young's modulus (GPa)	E_1= 207	$E_2 = E_3$ = 20.7	$E_r = (1-\alpha)E_r^0 + \alpha E_r^\infty$	
				E_r^0 = 3.447e-3	E_r^∞ = 3.447
5	Poisson's ratio	$\nu_{12} = \nu_{13}$=0.2	ν_{23}=0.3	$\nu_r = 0.35$	
6	Shear modulus (GPa)	$G_{12} = G_{13}$=27.6	G_{23}=7.96	$G_r = E_r/2(1+\nu_r)$	
7*	CTE ($℃^{-1}$)	CTE_1 = -9e-7	$CTE_2 = CTE_3$ = 7.2e-6	CTE_r = 5.76e-5	
8*	Total specific volume shrinkage	---		V_{sh}^T = 0.03	
9	Resin volumetric shrinkage	---		$e_V = \alpha V_{sh}^T$	

A2. Kinetic and material models

	Property	**Expression, parameters**	**Values**
1*	Cure kinetics model	$\frac{d\alpha}{dt} = \begin{cases} (B_1 + \alpha B_2)(1-\alpha)(\alpha_{crit} - \alpha), & \alpha \le 0.3 \\ B_3(1-\alpha), & 1 \ge \alpha \ge 0.3 \end{cases}$ Where $B_i = A_i e^{\frac{\Delta E_i}{RT}}$ Parameters: A_i, ΔE_i	$A_1(min^{-1})$ = 2.1e9 $A_2(min^{-1})$ = -2.01e9 $A_3(min^{-1})$ = 1.96e5 $\Delta E_1(J/mol)$ = 8.07e4 $\Delta E_2(J/mol)$ = 7.78e4 $\Delta E_3(J/mol)$ = 5.66e4

2	Viscosity model	$\mu = \mu_\infty e^{(U/RT)} e^{k\alpha}$ $if\ \mu > \mu_{max}\ then\ \mu = \mu_{max}$	$\mu_\infty(Pa.s)$ =7.93e-14 $U\ (J/mol) = 9.08e4$ $k = 14.1$
3	Instantaneous glass transition Tg	$T_g = T_{g0} + \frac{(T_{g\infty} - T_{g0})\lambda\alpha}{1-(1-\lambda)\alpha}$	$T_{g0}(℃) = 10.344$ $T_{g\infty}(℃) = 200.24$ $\lambda = 0.4$
4	Modulus development model	$E_r = \begin{cases} E_r^0, & \alpha \le \alpha_1 \\ (1-\alpha_{mod})E_r^0 + \alpha_{mod}E_r^\infty + \gamma\alpha_{mod}(1-\alpha_{mod})(E_r^\infty - E_r^0), & \alpha_1 \le \alpha \le \alpha_2 \\ E_r^\infty, & \alpha > \alpha_2 \end{cases}$ $\alpha_{mod} = \frac{\alpha - \alpha_1}{\alpha_2 - \alpha_1}$	$\alpha_1 = 0.0$ $\alpha_2 = 1.0$ $E_r^0\ (GPa) = 3.447e-3$ $E_r^\infty\ (GPa) = 3.447$ $\gamma = 0.0$
5	Chemical shrinkage model	$V_r^s = \begin{cases} 0.0 & \alpha \le \alpha_1 \\ A\alpha_s + (V_r^{s\infty} - A)\alpha_s^2 & \alpha_1 \le \alpha \le \alpha_2 \\ V_r^{s\infty}, & \alpha \ge \alpha_2 \end{cases}$ $\alpha_s = \frac{\alpha - \alpha_1}{\alpha_2 - \alpha_1}$ $\varepsilon_r^s = (1 + V_r^s)^{1/3} - 1$	$\alpha_1 = 0.0$ $\alpha_2 = 0.23$ $V_r^{s\infty}\ (m/m) = 0.03$ $A\ (m/m) = 0.03$

A3. Micromechanics model

A3.1 Engineering constants

The micromechanics equations for engineering constants of transversely isotropic lamina are provided here. Accordingly, the longitudinal young's modulus if given as:

$$E_1 = E_{1f}\nu_f + E_{1m}(1-\nu_f) + \frac{4(\nu_{12m}-\nu_{12f}^2)k_f k_m G_{23m}(1-\nu_f)\nu_f}{(k_f+G_{23m})k_m+(k_f-k_m)G_{23m}\nu_f}$$

Where subscript f stands for the fiber whereas subscript m stands for the matrix.

The major Poisson's ratio is given as:

$$\nu_{12} = \nu_{13} = \nu_{12f}\nu_f + \nu_{12m}(1-\nu_f) + \frac{(\nu_{12m}-\nu_{12f})(k_m-k_f)G_{23m}(1-\nu_f)\nu_f}{(k_f+G_{23m})k_m+(k_f-k_m)G_{23m}\nu_f}$$

The in-plane shear modulus is given as:

$$G_{12} = G_{13} = G_{12m}\frac{(G_{12f}+G_{12m})+(G_{12f}-G_{12m})\nu_f}{(G_{12f}+G_{12m})-(G_{12f}-G_{12m})\nu_f}$$

The transverse shear modulus is given as:

$$G_{23} = \frac{G_{23m}\left[k_m\left(G_{23m} + G_{23f}\right) + 2G_{23m}G_{23f} + k_m(G_{23f} - G_{23m})\nu_f\right]}{k_m\left(G_{23m} + G_{23f}\right) + 2G_{23m}G_{23f} - (k_m + 2G_{23m})(G_{23f} - G_{23m})\nu_f}$$

The transverse Young's modulus is given as:

$$E_2 = E_3 = \frac{1}{(1/4k_T) + (1/4G_{23}) + (\nu_{12}^2/E_1)}$$

Where k_T is the effective plane strain bulk modulus of the composite given by:

$$k_T = \frac{\left(k_f + G_{23m}\right)k_m + (k_f - k_m)G_{23m}\nu_f}{\left(k_f + G_{23m}\right) - (k_f - k_m)\nu_f}$$

The transverse Poisson's ratio is given as:

$$\nu_{23} = \frac{2E_1k_T - E_1E_2 - 4\nu_{12}^2k_TE_2}{2E_1k_T}$$

A3.2 Expansional strains

The micromechanical extensional strain equations are used to calculate the coefficients of thermal expansion (α_i) and chemical shrinkage (CSC_i). The expansion strain in the longitudinal direction ($i = 1$) is given as:

$$\epsilon_1 = \frac{\epsilon_{1f}E_{1f}V_f + \epsilon_{1m}E_{1m}(1 - V_f)}{E_{1f}V_f + E_{1m}(1 - V_f)}$$

And the expansional strain in the transverse direction ($i = 2$) is given as:

$$\epsilon_2 = (\epsilon_{2f} + \nu_{12f}\epsilon_{1f})V_f + (\epsilon_{2m} + \nu_{12m}\epsilon_{1m})\left(1 - V_f\right)$$

$$-[\nu_{12f} + \nu_{12m}(1 - \nu_f)]\left[\frac{\epsilon_{1f}E_{1f}V_f + \epsilon_{1m}E_{1m}(1 - V_f)}{E_{1f}V_f + E_{1m}(1 - V_f)}\right]$$

Where expansional thermal strains are obtained from the expansional strain expressions as $\alpha_i = \epsilon_i$, and the constituent thermal strains in the fiber and matrix are given as ϵ_{if}=CTE_{if}, $\epsilon_{im} = CTE_r$. Similarly, expansional chemical shrinkage strains are obtained as $CSC_i = \epsilon_i$, and the constituent chemical shrinkage strains in the fiber and matrix are given as ϵ_{if}= 0, $\epsilon_{im} = 1$.

A4. Optimization charts: Result charts for Run R12

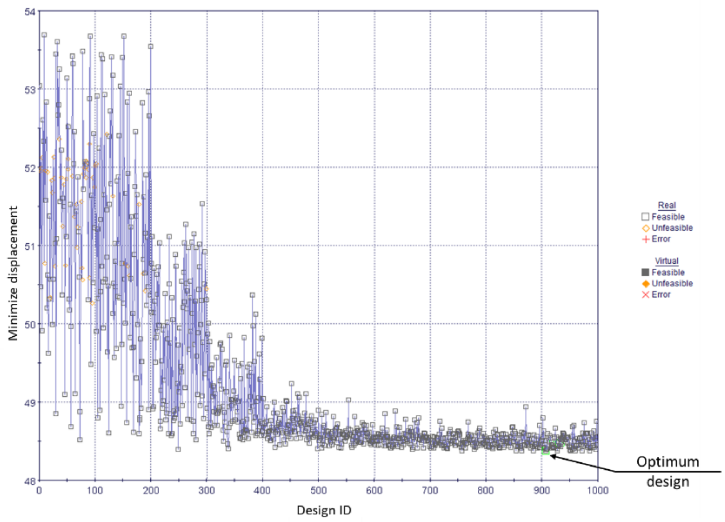

Figure A4.1 History chart of objective function (minimize displacement) for Run R12. The optimal design is marked by green box

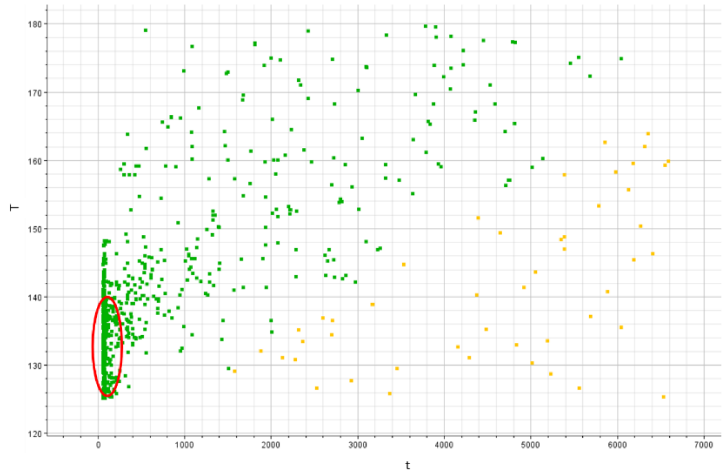

Figure A4.2 Time-temperature scatter plot for Run R12. The red circle shows higher density of iterations suggesting convergence of input variables t and T in that region. Yellow points represent infeasible design while green points represent feasible designs.

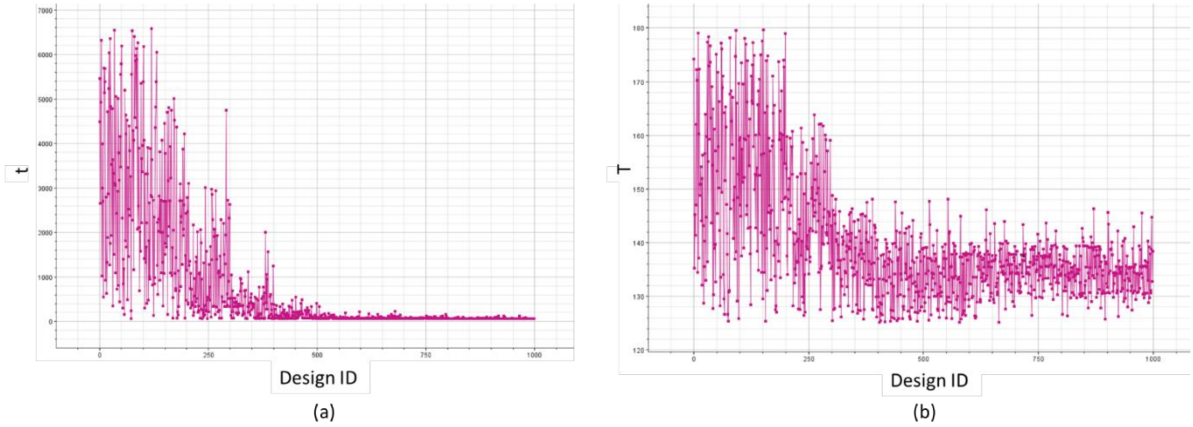

Figure A4.3 History plot of input variable a) time *t* and b) temperature *T* for Run R12.